Exotic properties of a voltage-gated proton channel from the snail *Helisoma trivolvis*

Sarah Thomas[1], Vladimir V. Cherny[2], Deri Morgan[2], Liana R. Artinian[3], Vincent Rehder[3], Susan M.E. Smith[1], and Thomas E. DeCoursey[2]

Voltage-gated proton channels, H_V1, were first reported in *Helix aspersa* snail neurons. These H^+ channels open very rapidly, two to three orders of magnitude faster than mammalian H_V1. Here we identify an H_V1 gene in the snail *Helisoma trivolvis* and verify protein level expression by Western blotting of *H. trivolvis* brain lysate. Expressed in mammalian cells, HtH_V1 currents in most respects resemble those described in other snails, including rapid activation, 476 times faster than hH_V1 (human) at pH_o 7, between 50 and 90 mV. In contrast to most H_V1, activation of HtH_V1 is exponential, suggesting first-order kinetics. However, the large gating charge of ∼5.5 e_0 suggests that HtH_V1 functions as a dimer, evidently with highly cooperative gating. HtH_V1 opening is exquisitely sensitive to pH_o, whereas closing is nearly independent of pH_o. Zn^{2+} and Cd^{2+} inhibit HtH_V1 currents in the micromolar range, slowing activation, shifting the proton conductance–voltage (g_H-V) relationship to more positive potentials, and lowering the maximum conductance. This is consistent with HtH_V1 possessing three of the four amino acids that coordinate Zn^{2+} in mammalian H_V1. All known H_V1 exhibit ΔpH-dependent gating that results in a 40-mV shift of the g_H-V relationship for a unit change in either pH_o or pH_i. This property is crucial for all the functions of H_V1 in many species and numerous human cells. The HtH_V1 channel exhibits normal or supernormal pH_o dependence, but weak pH_i dependence. Under favorable conditions, this might result in the HtH_V1 channel conducting inward currents and perhaps mediating a proton action potential. The anomalous ΔpH-dependent gating of HtH_V1 channels suggests a structural basis for this important property, which is further explored in this issue (Cherny et al. 2018. *J. Gen. Physiol.* https://doi.org/10.1085/jgp.201711968).

Introduction

Voltage-gated proton channels, H_V1, remain relative newcomers to the ion channel family. Although the idea of a depolarization-activated proton-selective ion channel was proposed in 1972 by J. Woodland Hastings and colleagues (Fogel and Hastings, 1972), the first voltage-clamp study that established the existence of this channel type occurred a decade later in the snail *Helix aspersa* (Thomas and Meech, 1982). An H_V1 gene was not identified until 2006 (Ramsey et al., 2006; Sasaki et al., 2006). Strong interest in this channel has arisen for two main reasons. First, its structure, with just four transmembrane helices, closely resembles the voltage-sensing domain of other voltage-gated ion channels, making it a unique model for voltage-gating mechanisms. By combining voltage sensing, gating, and conduction into a single module, H_V1 uniquely provides a direct readout of its gating state. Second, exceedingly diverse functions have been identified for H_V1 in many species and in many human tissues (DeCoursey, 2013).

The first systematic voltage-clamp characterization of voltage-gated proton currents was in *Lymnaea stagnalis* snail

neurons (Byerly et al., 1984). When mammalian proton currents were identified a decade later (DeCoursey, 1991), the most obvious difference was that H_V1 in snails activated two to three orders of magnitude faster. Here, we investigate the properties of the *Helisoma trivolvis* snail H_V1 gene product. We searched a transcriptome of *H. trivolvis* and found a putative HtH_V1; we then cloned the gene from a cDNA pool constructed from *H. trivolvis* brain tissue. We find many similarities to native proton currents studied in situ in other snail species, including rapid gating kinetics and other significant differences from mammalian H_V1. HtH_V1 currents differ from mammalian H_V1 in having exponential (vs. sigmoid) activation, similarity of τ_{act} and τ_{tail} at overlapping voltages, and maximal time constants near the midpoint of the proton conductance–voltage (g_H-V) relationship, all features suggestive of simple first-order gating kinetics expected of a monomeric protein. However, the existence of an extensive coiled-coil motif in the C terminus together with steep voltage dependence suggests "cooperative" gating of a dimeric protein. Potent

[1]Department of Molecular and Cellular Biology, Kennesaw State University, Kennesaw, GA; [2]Department of Physiology & Biophysics, Rush University, Chicago, IL; [3]Department of Biology, Georgia State University, Atlanta, GA.

Correspondence to T.E. DeCoursey: tdecours@rush.edu.

Check for updates

inhibition of HtH$_V$1 by Zn^{2+} and Cd^{2+} is explained by conservation of three of four members of the Zn^{2+}-binding site (Takeshita et al., 2014). The most remarkable property of the HtH$_V$1 channel is that its sensitivity to pH$_i$ is anomalously weak. The voltage-gating mechanism of all H$_V$1 identified to date is unique in being nearly equally responsive to pH$_o$ and pH$_i$, such that a one-unit change in either shifts the g_H-V relationship by 40 mV. This "rule of forty" (DeCoursey, 2013) has the biologically crucial effect of ensuring that H$_V$1 channels open only when there is an outward electrochemical gradient for H$^+$. In other words, H$_V$1 channels open only when doing so will result in acid extrusion from cells. Extensive mutation of hH$_V$1 has failed to produce any significant violation of the rule of forty (Ramsey et al., 2010; DeCoursey, 2016). In this issue, Cherny et al. identify a single amino acid difference between HtH$_V$1 and hH$_V$1 that appears to be responsible for the anomalous ΔpH dependence of the snail channel.

Materials and methods

Snail tissue
H. trivolvis, a pulmonate snail (order: Basommatophora; family: Planorbidae) from an albino stock maintained and continuously bred in aquaria at Georgia State University, was used for experiments. Snails were originally caught in the wild and introduced as an experimental model animal by S.B. Kater (Kater, 1974).

Gene cloning, mutagenesis, antibody synthesis, and Western blotting
Basic Local Alignment Search Tool searches of a transcriptome from *H. trivolvis* (unpublished data) yielded a hit that matched the criteria for an H$_V$1 sequence (Smith et al., 2011). Brains were dissected from *H. trivolvis* (Cohan et al., 2003), RNA was extracted from brain tissue using the RNeasy kit (Qiagen), and a cDNA pool was constructed using the SuperScript III kit (Life Technologies) according to the manufacturer's instructions. Primers designed against the transcriptome hit were used to clone the putative HtH$_V$1 coding sequence; the sequence was confirmed by commercial sequencing (SourceBio Science). This coding sequence was subcloned into eukaryotic expression vector pCA-IRES-eGFP. Site-directed mutagenesis of HtH$_V$1 was performed and sequence verified commercially (Genewiz). Antibody was raised in rabbit to a synthetic peptide (RSPSDHGEGFEEPLC) based on the predicted HtH$_V$1 epitope and affinity purified (Genscript) with a final concentration of 0.904 mg/ml. Total lysate was prepared from *H. trivolvis* brains that had been stored whole in Qiagen RLT buffer at –80°C for 12 mo. Brains were thawed and triturated briefly on ice; the lysate was cleared by centrifugation at 10,000 × g for 5 min. Proteins from *H. trivolvis* brain lysate were separated by SDS-PAGE, Western blotted, and probed with anti-HtH$_V$1 antibody (diluted 1:10,000 in blocking buffer) either alone or preincubated with 1,000-fold molar excess of synthetic peptide corresponding to the epitope.

Electrophysiology
HEK-293 cells were grown to ∼80% confluence in 35-mm culture dishes. HEK-293 cells were transfected with 0.4–0.5 μg cDNA using Lipofectamine 2000 (Invitrogen) or polyethylenimine (Sigma).

Plasmids that did not include GFP were cotransfected with GFP. After 24 h at 37°C in 5% CO$_2$, cells were trypsinized and replated onto glass coverslips at low density for patch-clamp recording. We selected green cells under fluorescence for recording. Because HEK-293 cells often have small endogenous H$_V$1 currents (Musset et al., 2011), cells that exhibited small currents suspected to be native were exposed to 1 μM Zn^{2+}, which has generally weaker effects on HtH$_V$1 (20% slowing of τ_{act}, ∼5 mV shift of the g_H-V relationship, and a 24% decrease in $g_{H,max}$ in three to four cells at pH$_o$ 7) than on hH$_V$1 (more than a twofold slowing of τ_{act}, ∼20 mV shift of the g_H-V relationship; Musset et al., 2010b). Cells determined on this basis to exhibit native currents were excluded from the study.

Micropipettes were pulled using a Flaming Brown automatic pipette puller (Sutter Instruments) from Custom 8520 Patch Glass (equivalent to Corning 7052 glass; Harvard Apparatus), coated with Sylgard 184 (Dow Corning Corp.), and heat polished to a tip resistance range of typically 3–10 MΩ with highly buffered TMA$^+$ pipette solutions. Electrical contact with the pipette solution was achieved by a thin sintered Ag-AgCl pellet (In Vivo Metric Systems) attached to a Teflon-encased silver wire, or simply a chlorided silver wire. A reference electrode made from a Ag-AgCl pellet was connected to the bath through an agar bridge made with Ringer's solution. The current signal from the patch clamp (EPC-9 from HEKA Instruments or Axopatch 200B from Axon Instruments) was recorded and analyzed using Pulse and PulseFit software (HEKA Instruments), or P-CLAMP software supplemented by Sigmaplot (SPSS). Seals were formed with Ringer's solution (in mM: 160 NaCl, 4.5 KCl, 2 CaCl$_2$, 1 MgCl$_2$, 5 HEPES, pH 7.4) in the bath, and the potential was zeroed after the pipette was in contact with the cell. Current records are displayed without correction for liquid junction potentials.

Whole-cell or excised inside-out patch configurations of the patch-clamp technique were performed. Bath and pipette solutions were used interchangeably. They contained (in mM) 2 MgCl$_2$, 1 EGTA, 80–100 buffer, and 75–120 TMA$^+$ CH$_3$SO$_3^-$, adjusted to bring the osmolality to ∼300 mOsm, and were titrated using TMAOH. Buffers with pK_a near the desired pH were used: homo-PIPES for pH 4.5–5.0, Mes for pH 5.5–6.0, Bis-Tris for pH 6.5, *N,N*-bis(2-hydroxyethyl)-2-aminoethanesulfonic acid for pH 7.0, HEPES for pH 7.5, Tricine for pH 8.0, and *N*-cyclohexyl-2-aminoethanesulfonic acid for pH 9.0. Experiments were done at room temperature (∼20–25°C). Current records are shown without leak correction.

Reversal potentials (V_{rev}) in most cases were determined from the direction and amplitude of tail current relaxation over a range of voltages after a prepulse that activated the proton conductance, g_H. When the g_H was activated negative to V_{rev}, the latter could be determined directly from families of currents. Currents were fitted with a single exponential to obtain the activation time constant (τ_{act}), and the fitted curve was extrapolated to infinite time to obtain the steady-state current amplitude (I_H), from which the g_H was calculated as $g_H = I_H/(V - V_{rev})$. Thus we assume that the time-dependent component reflects H$^+$ current, and time-independent current represents leak. Because of the strong voltage dependence of activation kinetics, we frequently applied longer pulses near threshold voltages and shorter pulses for large depolarizations to resolve kinetics and avoid proton

depletion associated with large H^{+} flux. The voltage at which g_H was 10% of $g_{H,max}$ ($V_{gH,max/10}$) was determined after defining $g_{H,max}$ as the largest g_H measured.

Results

HtH$_V$1 is a voltage-gated proton-selective channel

The gene coding for a putative voltage-gated proton channel was identified based on criteria established previously, namely the presence of four transmembrane helices homologous to S1–S4 of voltage sensor domains with an Asp in the middle of the S1 transmembrane helix and the RxWRxxR motif in S4 (Musset et al., 2011; Smith et al., 2011). We cloned the putative HtH$_V$1 gene from a cDNA pool of brain tissue, verifying that this gene is expressed at the RNA level. Protein level expression was verified by Western blotting of *H. trivolvis* brain lysate probed with a commercially raised antibody to a synthetic peptide based on a HtH$_V$1 epitope (Fig. 1, inset). The single protein detected ran at ~50 kD, somewhat larger than the predicted size of 40 kD. Glycosylation at the five putative N-glycosylation sites in the S1–S2 linker could account for this discrepancy, given that N-linked oligosaccharides range from 1,884 to 2,851 D (Imperiali and O'Connor, 1999). Excess synthetic peptide abolished the binding of antibody to brain lysate, establishing the specificity of the antibody. The antibody did not significantly bind to two proteins that do not contain the epitope: human glutathione S-transferase and luciferin binding protein from *Lingulodinium polyedrum*.

The HtH$_V$1 channel protein (Fig. 1) is substantially larger than the human hH$_V$1, with 360 amino acids (hH$_V$1 has 273). Much of this excess resides in the S1–S2 extracellular linker with 73 residues (vs. eight in hH$_V$1), which contains five potential N-glycosylation sites (vs. 0 in hH$_V$1). Focusing on the transmembrane regions, HtH$_V$1 has charged amino acids nearly identical to those of hH$_V$1. One exception is at the outer end of the S1 helix, where hH$_V$1 has basic Lys[125] but snail HtH$_V$1 has acidic Glu[120]. There is extensive predicted coiled-coil in the C terminus: 36 residues (positions 289–324) with 90% stringency, and 28 residues (294–321) with 99% stringency according to MARCOIL (Delorenzi and Speed, 2002). H$_V$1 in several species have been shown to exist as dimers, largely because of coiled-coil interactions in the C terminus (Koch et al., 2008; Lee et al., 2008; Tombola et al., 2008).

The HtH$_V$1 gene was transfected into HEK-293 cells. Under voltage clamp, transfected cells displayed depolarization-activated currents. The selectivity of these currents was established by measuring the reversal potential, V_{rev}, over a range of pH$_o$ and pH$_i$ values (Fig. 2). The measured values of V_{rev} are close to the Nernst potential for H^{+}, E_H, shown as a dashed line. Clearly, the HtH$_V$1 channel is highly proton selective over the pH range studied.

HtH$_V$1 gating is rapid with unusual voltage dependence

A family of currents generated by HtH$_V$1 at symmetrical pH 6.0 is illustrated in Fig. 3 A. The currents activate rapidly with depolarization, and activation becomes much faster at higher voltages. Although H$_V$1 currents in all species activate more rapidly at more positive voltages, the τ_{act} of HtH$_V$1 currents (solid and open red squares in Fig. 3 C) exhibits noticeably steeper voltage

dependence. The maximum slope of the τ_{act}-V relationship in seven cells at pH$_o$ 6 was 13.0 ± 3.4 mV/e-fold change in τ_{act} (mean ± SD). In several mammalian H$_V$1, τ_{act} changes e-fold in 40–72 mV (DeCoursey, 2003). Channel closing in HtH$_V$1 was also steeply voltage dependent (Fig. 3 B and blue diamonds in Fig. 3 C), with τ_{tail} changing e-fold in 14.2 ± 1.9 mV in six cells. In mammalian cells, the slope is typically much flatter, 26–44 mV/e-fold change in τ_{tail} (DeCoursey, 2003).

A remarkable feature of HtH$_V$1 is that at intermediate voltages where the measurements overlap, the time constants of H^{+} current turn-on (τ_{act}) and deactivation (τ_{tail}) essentially superimpose (Fig. 3 C). This behavior is suggestive of simple first-order kinetics, such as a two-state system:

$$ Closed \xrightarrow{\alpha} \underset{\beta}{\overset{}{\longleftarrow}} Open $$

(Scheme 1)
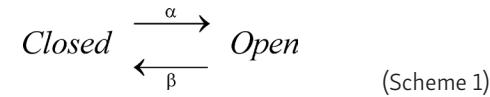
in which α is the rate of channel opening and β is the rate of channel closing, and the time constant τ is $(α + β)^{-1}$ (Hodgkin and Huxley, 1952). Another feature suggestive of first-order kinetics is evident in the g_H-V relationship from this cell (Fig. 3 D). The voltage at which the g_H is half-maximal is ~40 mV, where the time constants are maximal (Fig. 3 C). However, the limiting slope of the g_H-V relationship in Fig. 3 D, i.e., the slope of the most negative values obtained, indicates a gating charge of ~6 e_0. The mean gating charge in 18 limiting slope measurements was 5.5 ± 0.9 e_0 (mean ± SD). Because the range of g_H values resolved did not exceed three orders of magnitude, these gating charge estimates should be considered lower limits. In most species, cooperative gating of the dimeric H$_V$1 channel doubles the gating charge from 2–3 to 4–6 e_0 (Gonzalez et al., 2010, 2013; Fujiwara et al., 2012).

Mean gating kinetics determined at symmetrical pH 7.0 is shown in Fig. 4 A. As was also seen at pH 6.0 (Fig. 3 C), at voltages where τ_{act} and τ_{tail} overlap, they have similar values, suggestive of first-order gating kinetics. In the first description of proton currents in snail neurons, the activation time to half-peak current was 25 ms or less at pH$_o$ 7.4 (Byerly et al., 1984). With this in mind, the activation kinetics of HtH$_V$1 is quite similar to that reported in neurons from *L. stagnalis*. When proton currents were first identified in mammalian species, they were found to be radically slower (DeCoursey, 1991; Bernheim et al., 1993; DeCoursey and Cherny, 1993; Demaurex et al., 1993; Kapus et al., 1993). The activation kinetics of HtH$_V$1 is two to three orders of magnitude faster than that of hH$_V$1 (Fig. 4 B), averaging 476 times faster between 50 and 90 mV at pH$_o$ 7.

HtH$_V$1 is sensitive to inhibition by external Zn^{2+} and Cd^{2+}

The polyvalent metal cations Zn^{2+} and Cd^{2+} were among the first H$_V$1 inhibitors identified (Thomas and Meech, 1982; Mahaut-Smith, 1989b). Zn[2+] in particular has been used widely on H$_V$1 identified in new species and remains the most potent inhibitor (Cherny and DeCoursey, 1999). Fig. 5 illustrates the effects of 100 µM Zn[2+] or Cd[2+] on HtH$_V$1 currents. Three main effects are evident: the current amplitude is reduced, the current activates more slowly (scaled currents in Fig. 5 D), and the g_H-V relationship is shifted positively along the voltage axis. These three parameters are interrelated in that a positive shift of the
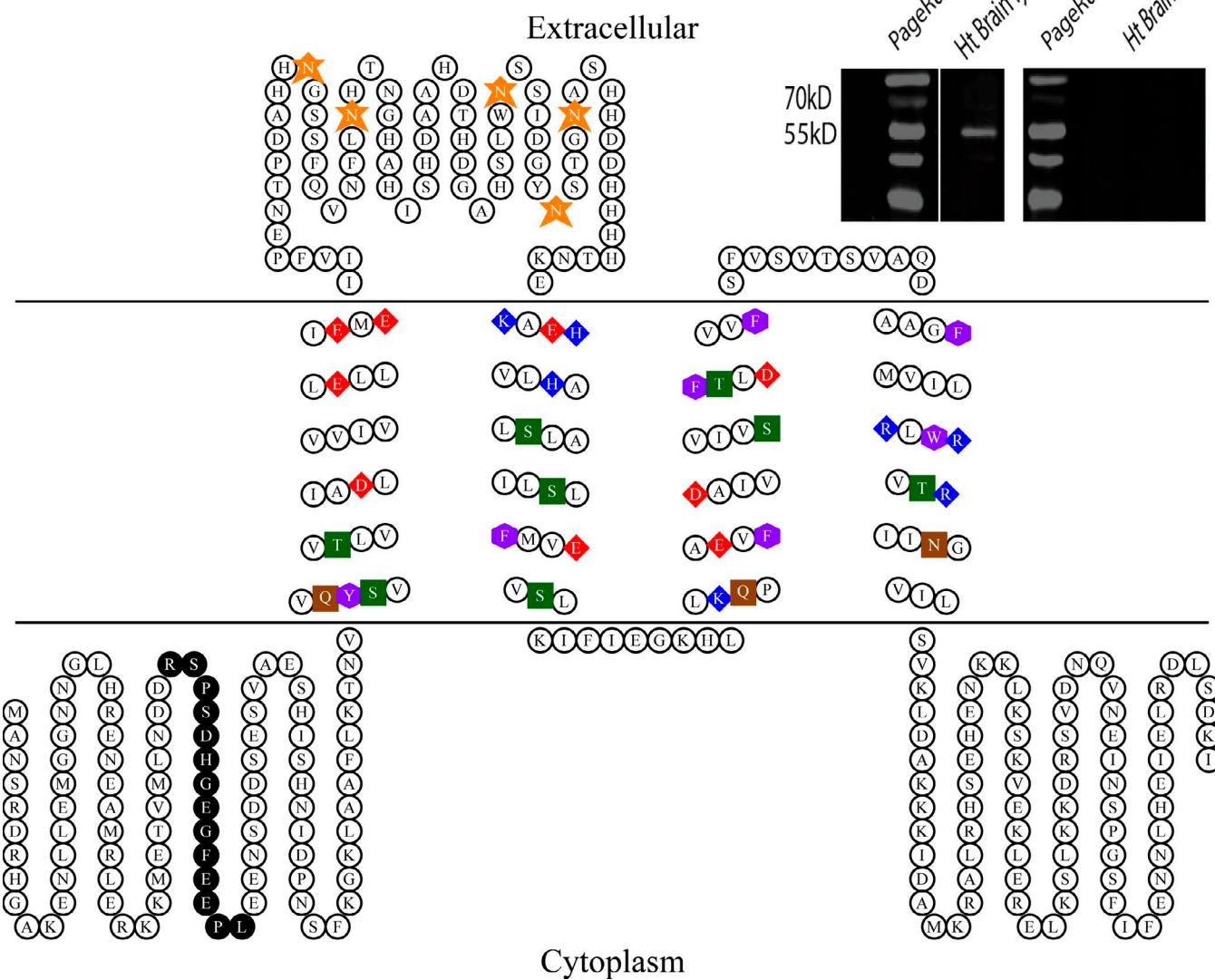
Figure 1. **The HtH$_V$1 proton channel sequence.** Topology of the HtH$_V$1 channel, with transmembrane regions defined by alignment with those determined for hH$_V$1 by electron paramagnetic resonance (Li et al., 2015). Amino acids in transmembrane regions are color coded as follows: red, acids; blue, bases; brown, amines; purple, aromatics; green, hydroxyls; and orange stars, putative (extracellular) glycosylation sites. Noteworthy are D107 in S1, which presumably confers H$^+$ selectivity, and the RxWRxxR motif in S4, both of which are conserved universally in all known H$_V$1. Sequence in black is the epitope used to generate antibody. Inset shows Western blots of *H. trivolvis* brain, confirming the presence of HtH$_V$1 protein. Drawn with TOPO2 (http://www.sacs.ucsf.edu/TOPO2/).

g_H-V relationship will in itself decrease the current and slow τ_{act} at any given voltage. The mean changes in these three parameters produced by 10 or 100 µM of the two metals are summarized in Fig. 5 E.

These three effects of polyvalent metal cations have been observed for H$_V$1 from many species. As in rat H$_V$1 (Cherny and DeCoursey, 1999), Zn^{2+} is more potent than Cd^{2+} in HtH$_V$1. Focusing on the three main effects, HtH$_V$1 was more sensitive, similar to, or less sensitive than human H$_V$1 (hH$_V$1). The reduction of $g_{H,max}$ is glaringly obvious for HtH$_V$1, whereas in mammalian H$_V$1 this effect is small and difficult to detect because of the interrelatedness of the three effects (Cherny and DeCoursey, 1999).

Zn^{2+} at 10 µM slows τ_{act} by four- to fivefold in both hH$_V$1 (Musset et al., 2010b) and HtH$_V$1 (Fig. 5). In contrast, the shift of the g_H-V relationship by Zn^{2+} is far more profound in human hH$_V$1, with a 20-mV shift produced by 1 µM Zn^{2+} (Musset et al., 2010b) compared with a 12-mV shift by 10 µM Zn^{2+} in HtH$_V$1 (Fig. 5).

Unique ΔpH dependence of HtH$_V$1 gating

Families of proton currents generated by the *H. trivolvis* proton channel gene product, HtH$_V$1, in a cell studied at four pH$_o$ values with pH$_i$ 6 are illustrated in Fig. 6 (A–D). The currents activate with depolarization, and activation becomes much faster at higher voltages. Both voltage dependence and kinetics were
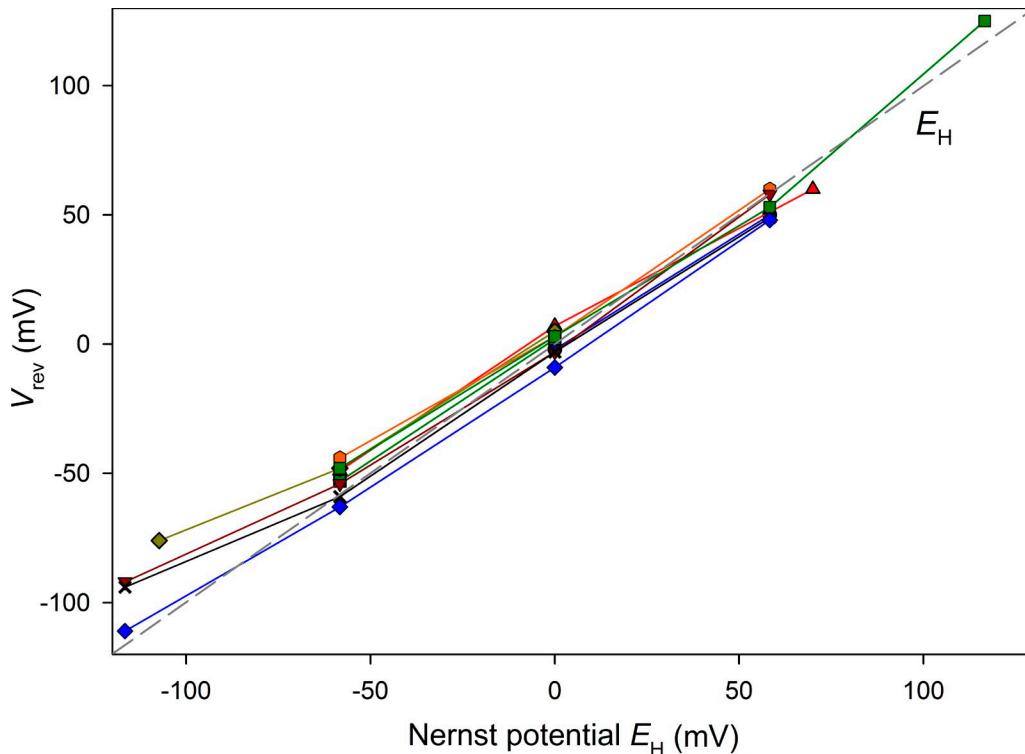
Figure 2. The HtH$_V$1 proton channel is highly proton selective. Reversal potentials (V_{rev}) were measured over a range of pH$_i$ (5.0–8.0) and pH$_o$ (4.8–8.0) values, as described in Materials and methods, in eight cells and one inside-out patch. Data from each cell or patch are connected by lines. The dashed gray line shows identity between V_{rev} and the Nernst potential for H$^+$, E_H, i.e., the expectation for perfect selectivity.

exquisitely sensitive to pH$_o$. At higher pH$_o$, the proton conductance, g_H, turned on at more negative voltages and turned on much more rapidly (note the different time bases). Fig. 6 (E–H) shows deactivation kinetics at each pH$_o$ during tail current measurements in this cell. Channel closing becomes much more rapid at more negative voltages.

In Fig. 6 I, time constants of H$^+$ current turn-on (activation, τ_{act}) and turn-off (deactivation, τ_{tail}) from the same cell are plotted. Several intriguing features emerge. Unlike H$_V$1 in other species, at intermediate voltages where τ_{act} and τ_{tail} overlapped, they were of similar magnitude (as was seen in Figs. 3 and 4). Because this behavior suggests first-order kinetics (Scheme 1), the data in Fig. 6 I were analyzed in this way, and the expressions for each rate constant are given on the graph in the following form:

$$\alpha(V) \ = \ \alpha e^{V/k_\alpha} \tag{1}$$

and

$$\beta(V) \ = \ \beta e^{-V/k_\beta}. \tag{2}$$

The voltage dependence of τ_{act} is steep (small k_α) and appears to become steeper at lower pH$_o$. The voltage dependence of channel closing, τ_{tail}, is also steep (small k_β) but appears to be independent of pH$_o$. To a first approximation, β is independent of pH$_o$, whereas α is markedly influenced by pH$_o$. Mean values for the rate constants are plotted in Fig. 7. Confirming the impression from Fig. 6 I (where k_α was 11.4, 18, 26, and 30 mV at pH$_o$ 5, 6, 7, and 8), k_α increased with pH$_o$, and k_β was pH independent.

But by far the strongest effect of pH is that increasing pH$_o$ massively increases the opening rate constant α, which increased more than an order of magnitude per unit increase in pH$_o$. Stated differently, protonation at the external face of the HtH$_V$1 channel strongly inhibits channel opening. More subtly, it is evident that for any given pH$_o$, α is higher and β is lower at pH$_i$ 6 than at pH$_i$ 7; hence, lower pH$_i$ both promotes opening and slows closing.

The g_H-V relationships from the cell in Fig. 6 (A–I) are plotted in Fig. 6 J. Like other H$_V$1, HtH$_V$1 exhibits robust pH$_o$-dependent shifts with increasing pH$_o$ shifting the g_H-V relationship negatively. The shifts for pH$_o$ 5 → 6 and 6 → 7 are closer to 50 than 40 mV, indicating that HtH$_V$1 exceeds the rule of forty for changes in pH$_o$. To reconstruct g_H-V relationships using the simple first-order assumption (Scheme 1 and Eqs. 1 and 2), which predicts that $P_{open} = \alpha/(\alpha + \beta)$, the solid curves in Fig. 6 J were drawn from the rate constant equations in Fig. 6 I scaled by $g_{H,max}$. Their limiting slope at negative voltages is shallower than observed. Squaring the P_{open}-V relationships, as in the classic Hodgkin–Huxley n^2 approach (Hodgkin and Huxley, 1952), produces the steeper dashed curves, which better approximate the data. Without pushing the model too far, we conclude that it is probable that, like several other H$_V$1 (Gonzalez et al., 2010; Musset et al., 2010b; Tombola et al., 2010; Fujiwara et al., 2012), HtH$_V$1 functions as a dimer in which both protomers must activate before either one conducts.

The effects of changes in pH$_i$ were explored in inside-out patches, as illustrated in Fig. 8. The resolution was limited somewhat by the typically small current amplitude combined with
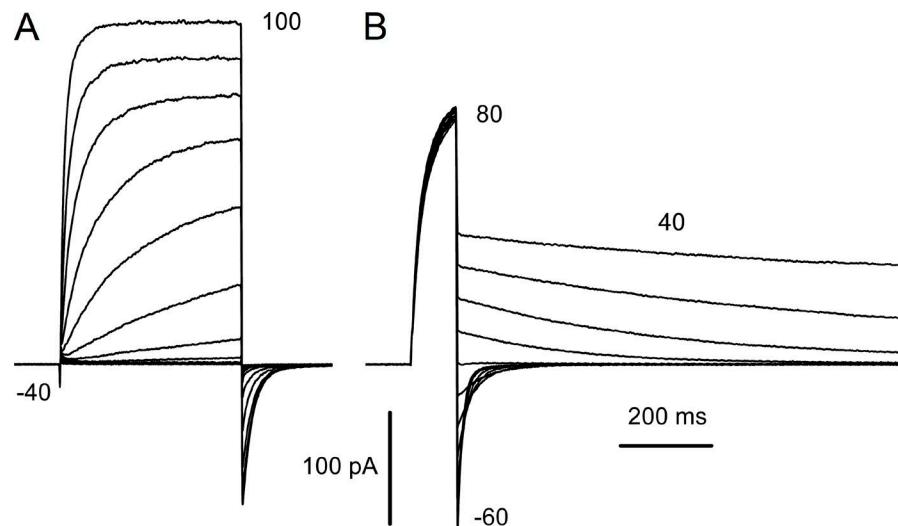
Figure 3. **Strong voltage dependence of HtH$_V$1 gating kinetics. (A)** A family of proton currents at pH$_o$ 6 and pH$_i$ 6 in a HEK-293 cell transfected with HtH$_V$1. Pulses were applied in 10-mV increments up to 100 mV from a holding potential, V_{hold} = –40 mV. **(B)** Tail currents in the same cell elicited by a prepulse to 80 mV, in 10-mV increments from –60 to 40 mV. **(C)** Gating kinetics in the same cell. The time constant of channel opening, τ_{act} (red squares) was obtained from single exponential fits to rising currents. Tail current (deactivation, channel closing) time constants, τ_{tail}, were also from single exponential fits. Open squares and dashed lines show τ_{act} from a second family. **(D)** The proton conductance was calculated from the extrapolated single exponential fits of currents and the measured V_{rev}.
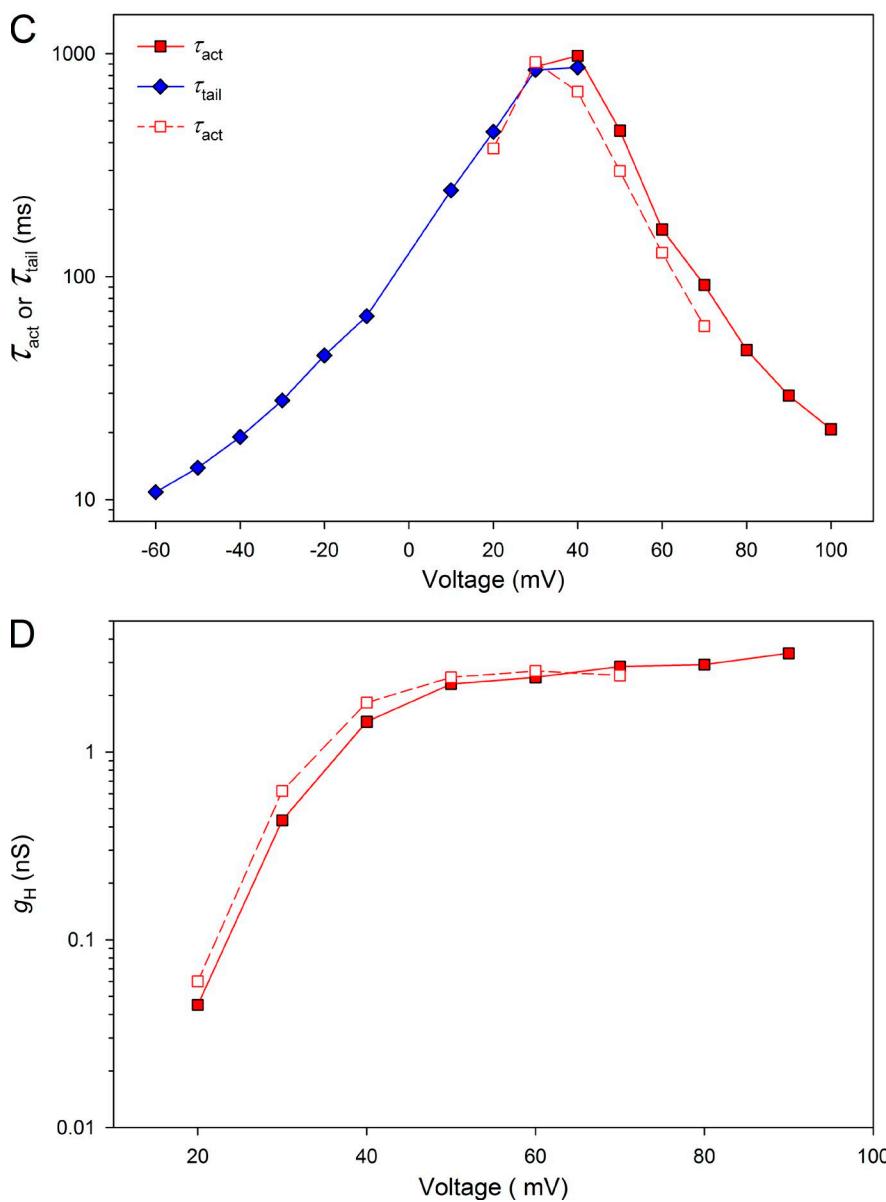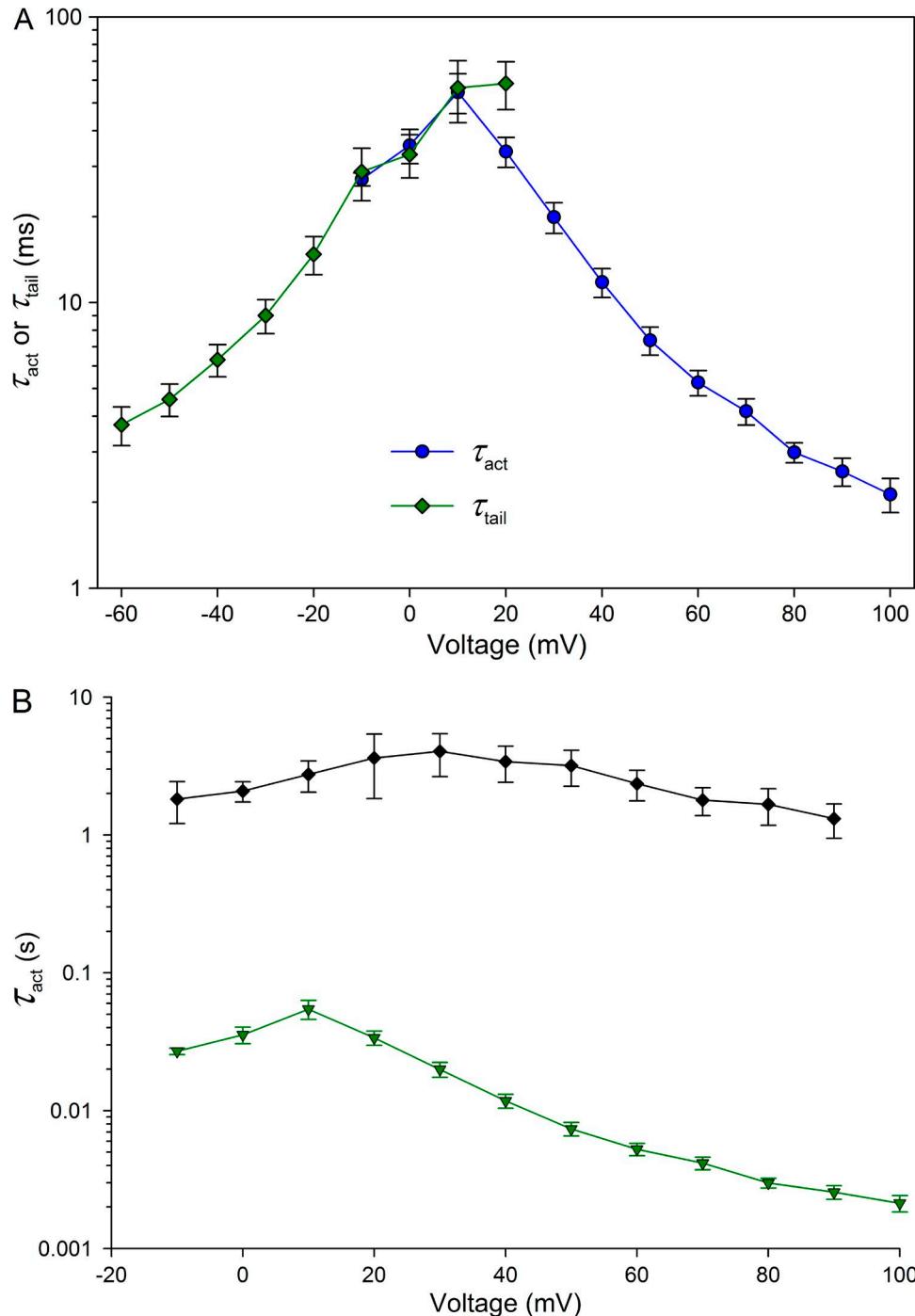
Figure 4.   **Activation and deactivation kinetics of HtH$_V$1 at symmetrical pH 7.0 (pH$_o$ 7, pH$_i$ 7) overlap. (A)** The time constant of channel opening, τ_{act}, was obtained from single exponential fits to currents during activation. Tail current (deactivation, channel closing) time constants, τ_{tail}, were also from single exponential fits. Error bars represent mean ± SEM for 7–17 cells for τ_{act} and 3–7 cells for τ_{tail}. **(B)** Comparison of channel opening kinetics in HtH$_V$1 and hH$_V$1. Activation time constants (τ_{act}) in WT HtH$_V$1 (triangles, from A) and WT hH$_V$1 (diamonds, from Cherny et al., 2015) at pH$_o$ 7, pH$_i$ 7. Error bars represent mean ± SEM.

rapid activation kinetics at some pH. Activation kinetics could be resolved at low but not at high pH$_i$. For example, at pH$_i$ 8 (Fig. 8 C), inward current is clearly activated, but the kinetics is ambiguous. Nevertheless, it is evident in Fig. 8 D that activation kinetics depends only weakly on pH$_i$, in stark contrast to the strong dependence seen for pH$_o$ (Figs. 6 and 7), and in contrast to mammalian H$_V$1, in which lowering pH$_i$ speeds activation fivefold/unit (DeCoursey and Cherny, 1995; Villalba-Galea, 2014).

Deactivation kinetics was poorly resolved in most patches. The most surprising feature (Fig. 8 E) is that the heretofore universal rule of forty governing ΔpH-dependent gating is violated by HtH$_V$1. Changing pH$_i$ shifts the g_H-V relationship of HtH$_V$1 by just 20 mV/unit or less. The aberrant behavior of HtH$_V$1 provides clues to the mechanism of ΔpH-dependent gating.

Fig. 9 summarizes the ΔpH dependence of HtH$_V$1. For a variety of reasons discussed elsewhere (Cherny et al., 2015), we
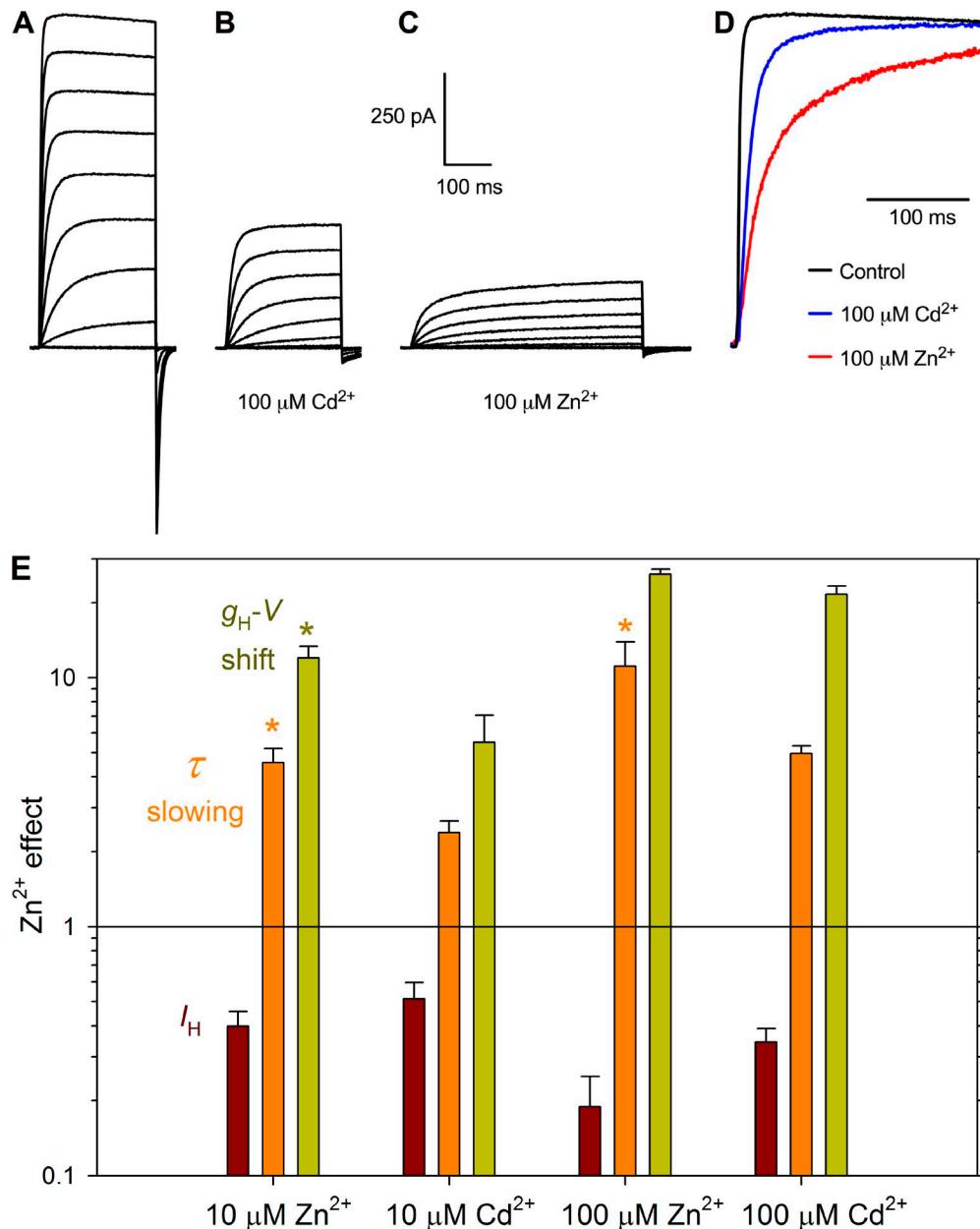
Figure 5. **HtH$_V$1 currents are moderately sensitive to inhibition by divalent metal cations. (A)** A family of HtH$_V$1 currents at pH$_o$ 7, pH$_i$ 7, in 10-mV increments up to 80 mV. **(B and C)** Families of currents in the same cell at the same voltages in the presence of 100 µM Cd^{2+} or 100 µM Zn^{2+}, respectively. Calibrations apply to A–C. **(D)** The currents at 80 mV from the three families in A–C are superimposed after scaling to the same maximum current and time base. **(E)** Three main effects of Zn^{2+} and Cd^{2+} are summarized: I_H (relative to 1) is the fractional current remaining at 60 mV in the presence of metal; τ slowing (also relative to 1) is the slowing of activation time constants (the ratio τ$_{act}$ [metal/control] at 80 mV); and g_H-V shift is the shift of $V(g_{H,max}/10)$. Mean ± SEM is plotted for four cells at 10 µM metal and five cells at 100 µM, all studied at pH$_o$ 7. In some cells, a second kinetic component appeared at high metal concentrations. In these cases, we used the faster of the two time constants for this comparison. *, Zn^{2+} effect is significantly greater than Cd^{2+} effect (P < 0.05 by Student's t test).

have adopted $V(g_{H,max}/10)$, the voltage at which the g_H is 10% of its maximal value, as a parameter to define the position of the g_H-V relationship. We find this preferable to other parameters that have been used for this purpose, such as the midpoint of a Boltzmann curve (which frequently does not fit the data well or is ill determined) or the threshold voltage at which current is first detectable (which is arbitrary, depends on the signal-to-noise ratio, and is particularly difficult to resolve when it occurs near V_{rev}, as frequently occurs in HtH$_V$1). It is evident in Fig. 9 that when pH$_o$ < 7, changes in pH$_o$ shift $V(g_{H,max}/10)$ by more than

40 mV/unit (for reference, this slope is shown as a dashed green line in Fig. 9). H$_V$1 in two other species (coccolithophore EhH$_V$1 and insect NpH$_V$1) also exhibit shifts with pH$_o$ greater than 40 mV/unit (Cherny et al., 2015; Chaves et al., 2016). At pH$_o$ higher than 7, the shift decreases, which may reflect saturation of the response caused by the ambient pH approaching the pK_a of a critical titratable group. Saturation of ΔpH dependence has been observed previously in hH$_V$1 at pH > 8 (Cherny et al., 2015).

The most striking result in Fig. 9 is the data for changes in pH$_i$ (dark red diamonds), which reveal that the position of the
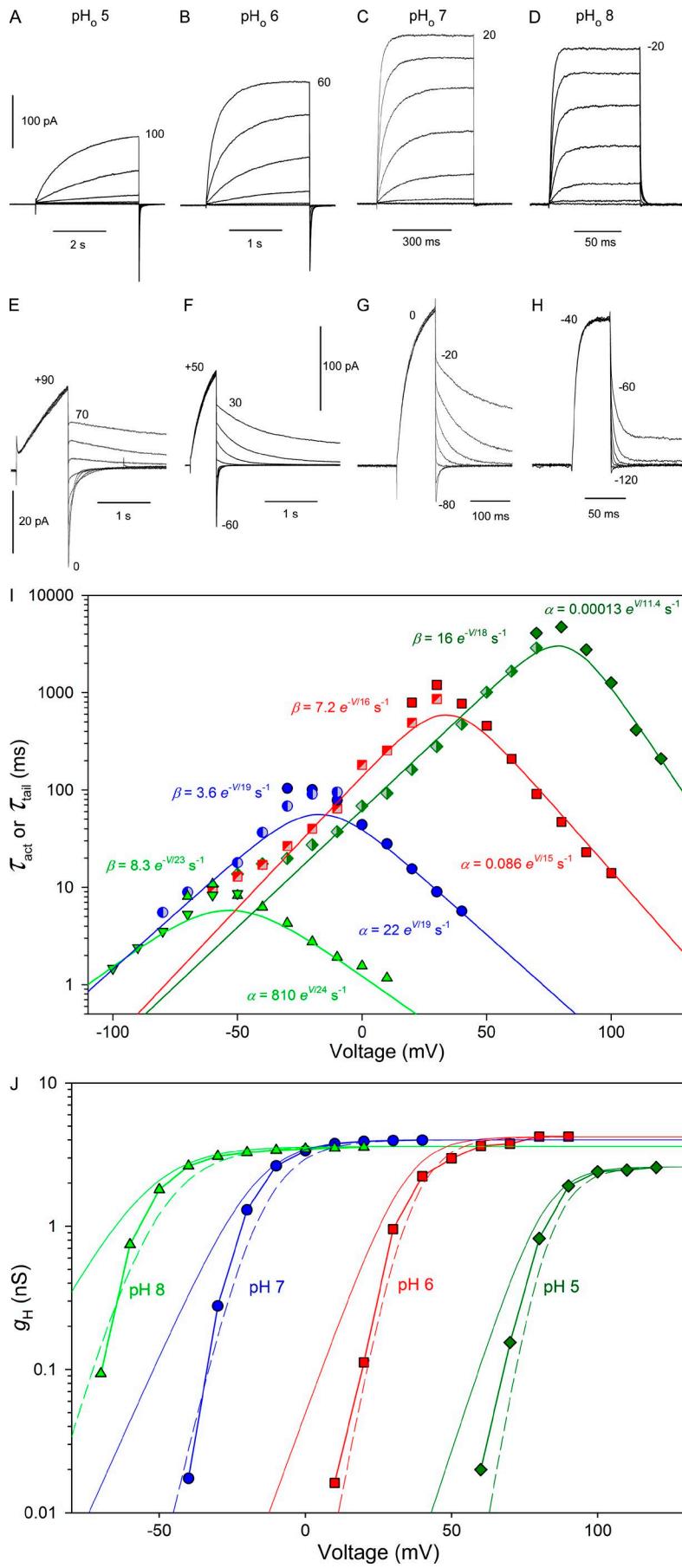
Figure 6. **Exquisite sensitivity of HtHv1 gating kinetics to pH$_o$.** **(A–D)** Families of proton currents at pH$_o$ 5, 6, 7, and 8 with pH$_i$ 6 in a HEK cell transfected with HtHv1. Pulses were applied in 10-mV increments from a holding potential, V_{hold} = –40 mV (A and B), –60 mV (C), or –90 mV (D) up to the voltage indicated. Note the different time calibrations. **(E–H)** Tail current measurements in the same cell at each pH$_o$. Tail currents were recorded in 10-mV increments over the voltage range indicated. V_{hold} is the same as in the top row, and the prepulse voltage is indicated. Current calibration in F also applies to G and H. **(I)** Dependence of gating kinetics on pH$_o$. At each pH$_o$ value, the solid symbols show τ_{act} from single exponential fits of currents during activation, and the half-filled symbols or inverted triangles show deactivation kinetics (τ_{tail}) during tail currents. Note that τ_{act} and τ_{tail} overlap, consistent with simple first-order kinetics, and both have steep voltage dependence. The curves are drawn from the rate constant equations given on the graph in I, where $\tau = 1/(\alpha + \beta)$. **(J)** g_H-V relationships measured in the same cell. Solid curves show P_{open}-V relationships calculated from the rate constants defined by the equations in I ($P_{open} = \alpha/(\alpha + \beta)$, scaled by $g_{H,max}$). The dashed curves show the prediction of a Hodgkin–Huxley n^2 model ($P_{open} = [\alpha/(\alpha + \beta)]^2$, scaled by $g_{H,max}$).

Thomas et al.
A snail proton channel with anomalous properties

Journal of General Physiology
https://doi.org/10.1085/jgp.201711967

843
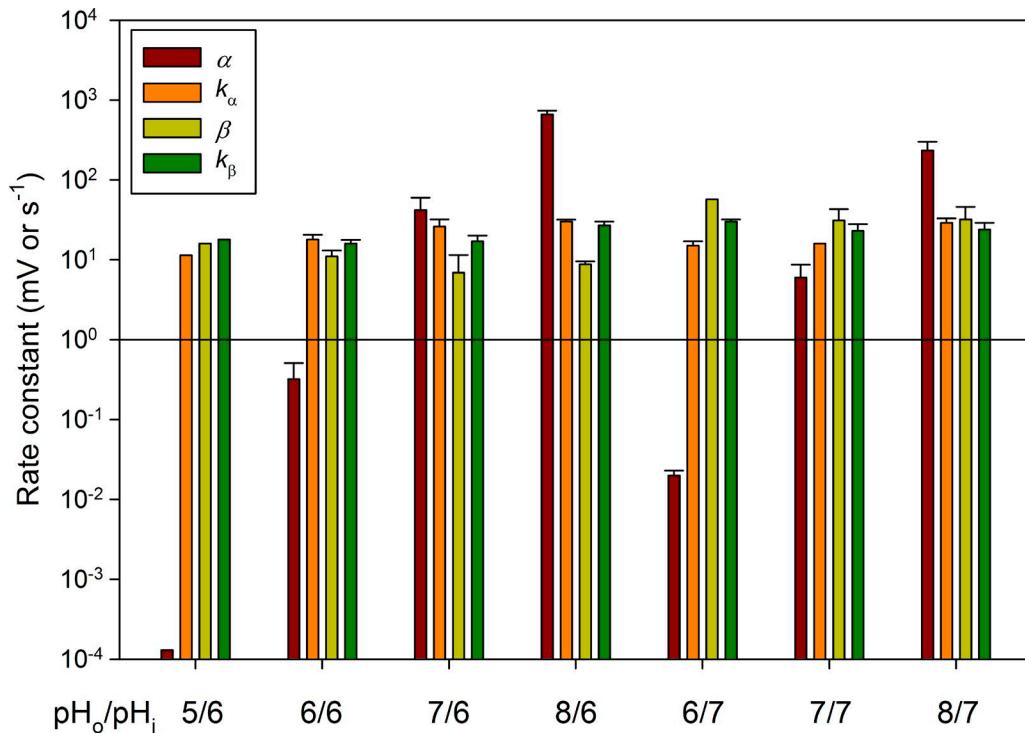
Figure 7. Rate constants extracted from fits of time-constant data at various pH values (pH$_o$/pH$_i$). Time constants were fitted to Eqs. 1 and 2, as illustrated in Fig. 6 I. Mean ± SEM plotted for n = 1–4.

g_H-V relationship depends only weakly on pH$_i$. There is no clear indication of saturation, although the slope appears to increase at larger ΔpH (i.e., lower pH$_i$). This is qualitatively like the whole-cell pH$_o$ response, which is steepest at low pH$_o$ and saturates at high pH$_o$. Over the entire ΔpH range, the mean slope is only 15.3 mV/unit change in pH$_i$. HtH$_V$1 is the first H$_V$1 in which such weak ΔpH dependence has been identified.

Discussion

The rapid kinetics of HtH$_V$1 resembles that of other snail proton channels but differs from mammalian H$_V$1

The snail H$_V$1, HtH$_V$1, exhibits all of the major features of H$_V$1 in all species studied thus far. It is highly proton selective and it is voltage gated, opening with depolarization, and opening more rapidly at more positive voltages. Furthermore, its voltage dependence is strongly modulated by pH, such that increasing pH$_o$ or decreasing pH$_i$ shifts the g_H-V relationship negatively, in what has been called ΔpH-dependent gating (Cherny et al., 1995). Beyond these qualitative similarities, however, HtH$_V$1 differs markedly from H$_V$1 in humans and other mammalian species. The main differences include very rapid activation kinetics, steeply voltage-dependent activation kinetics, activation in a more negative voltage range, exponential rather than sigmoid activation, and distinctly aberrant ΔpH dependence. These properties are discussed below.

The first voltage-gated proton channels to be characterized by voltage clamp were in neurons from the snails *L. stagnalis* (Byerly et al., 1984), *H. aspersa* (Thomas and Meech, 1982; Mahaut-Smith, 1989b), and *Helix pomatia* (Doroshenko et al., 1986). All activated

rapidly, with time constants, τ_{act}, of a few milliseconds. When mammalian proton currents were identified, the most obvious difference was much slower activation, with τ_{act} in the range of seconds (DeCoursey, 1991; Bernheim et al., 1993; Demaurex et al., 1993; Kapus et al., 1993) or even minutes (DeCoursey and Cherny, 1993). A more subtle difference was that mammalian H$_V$1 activate with a distinct delay, whereas snail H$_V$1 activate exponentially. We show here that the HtH$_V$1 channel shares both properties with other snail H$_V$1. Byerly et al. (1984) reported half-times for activation of less than 25 ms for proton currents in *L. stagnalis* neurons at pH$_o$ 7.4, as observed here at pH$_o$ 7 (Fig. 4 A).

Paradoxically, some aspects of gating in HtH$_V$1 suggest a simple first-order transition between closed and open states

Activation and deactivation time constants in HtH$_V$1 are of similar magnitude at voltages where they overlap. This property is typical of a simple first-order system (Scheme 1). In mammalian H$_V$1 (DeCoursey, 1991; Cherny et al., 1995, 2001; DeCoursey and Cherny, 1996, 1997; Cherny and DeCoursey, 1999; Schilling et al., 2002), activation tends to be slower than deactivation. This asymmetrical behavior is typical of cooperatively gated multimeric channels (Hodgkin and Huxley, 1952; Hille, 2001), because all subunits must activate before the channel conducts, whereas only one subunit needs to deactivate to close the pore. In rat H$_V$1, deactivation was rapid, pH$_o$ independent, and weakly voltage dependent at large negative voltages (Cherny et al., 1995). However, near the threshold voltage for g_H activation, a second slower component of τ_{tail} appeared that was pH$_o$ dependent and of comparable magnitude to τ_{act}. Also suggestive of a first-order system in HtH$_V$1 is that τ_{act} and τ_{tail} were slowest at the midpoint of the
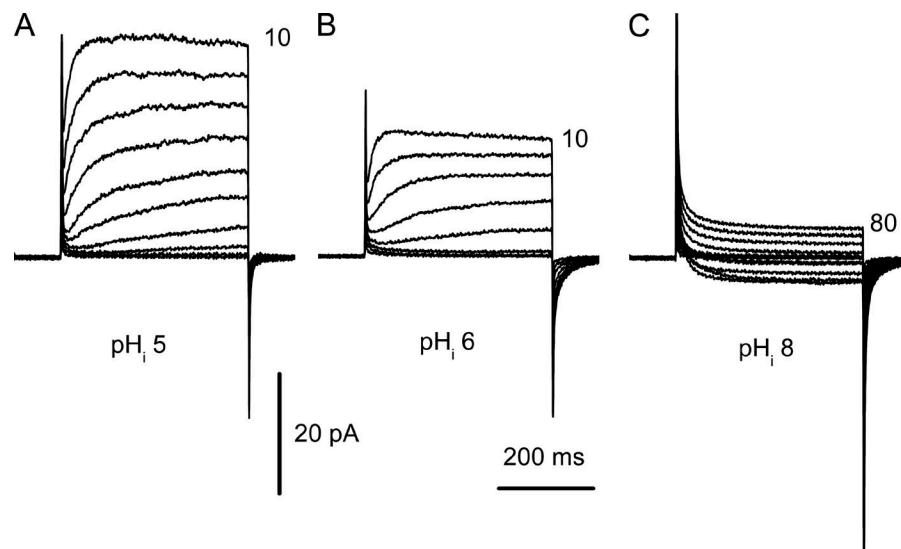
Figure 8. **Gating of proton currents in HtH$_V$1 in an inside-out patch at several pH$_i$ values.** **(A–C)** Current families at pH$_i$ 5, 6, and 8 in a patch with pH$_o$ 7. Pulses were applied in 10-mV increments up to the voltage indicated, from V_{hold} = –90 mV (A) or –70 mV (B and C). **(D)** Activation kinetics appears to be nearly independent of pH$_i$. **(E)** The dependence of the g_H-V relationship on pH$_i$ is weaker than in all other known H$_V$1. Currents were determined by extrapolation of single exponential fits for rising currents, or from steady-state currents when kinetics was inscrutable (e.g., at pH$_i$ 8).
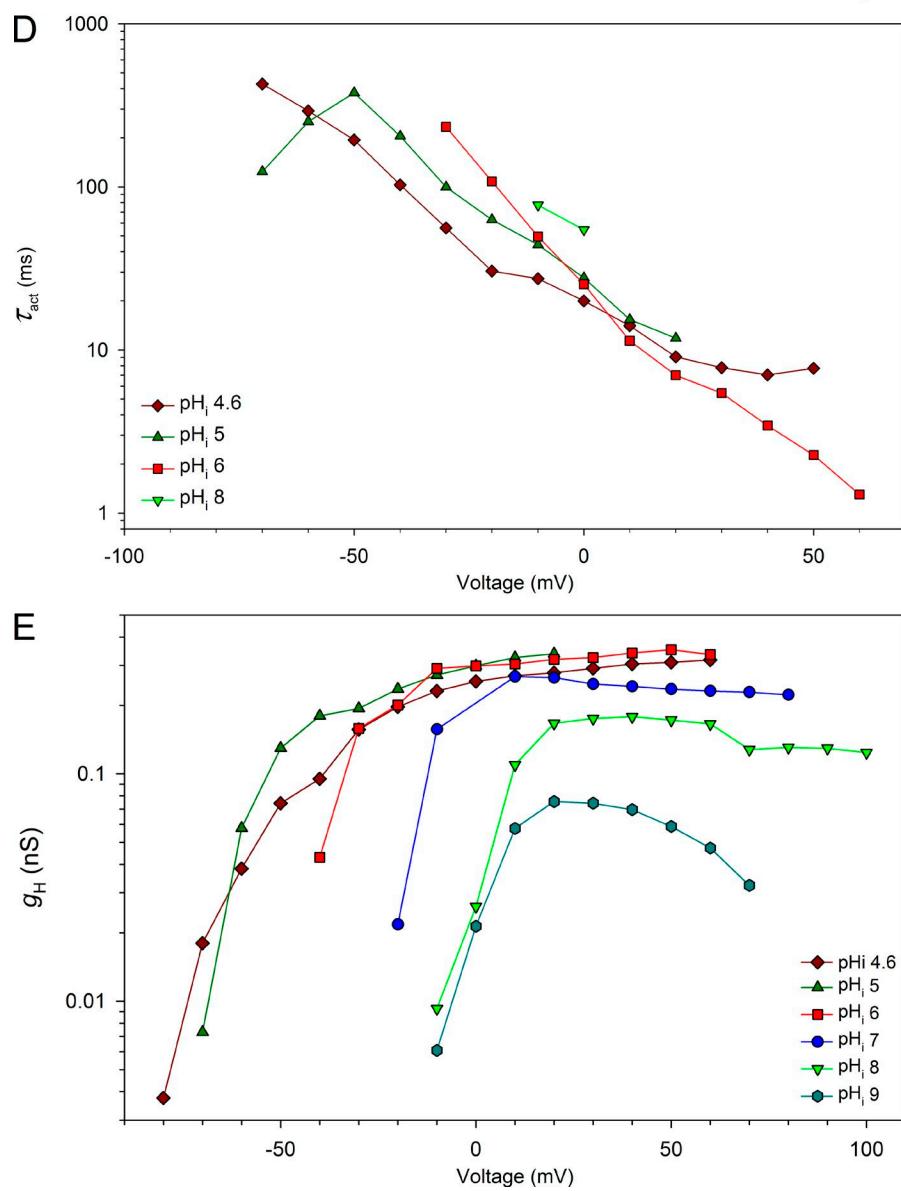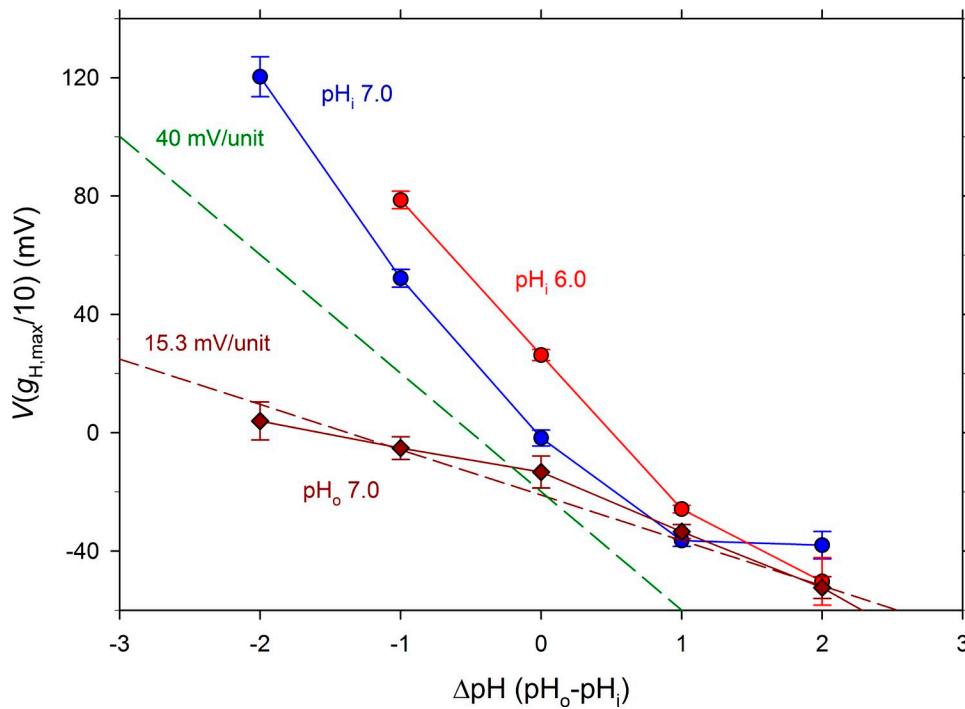
Figure 9. Anomalous ΔpH dependence of gating in HtH$_V$1. The position of the g_H-V relationship was defined in terms of $V(g_{H,max}/10)$, the voltage at which the g_H was 10% of $g_{H,max}$, the maximal value measured. In whole-cell measurements, pH$_o$ was varied, with mean ± SEM data for pH$_i$ 6 or 7 plotted separately. The slope of these data is well above 40 mV/unit (indicated as a dashed green line) and appears to begin to saturate above pH$_o$ 7 (ΔpH > 0 for pH$_i$ 7 and ΔpH > 1 for pH$_i$ 6). In contrast, when pH$_i$ was varied using inside-out patches, all with pH$_o$ 7, there was very little shift of the g_H-V relationship. The linear regression slope of the pH$_o$ 7 data is 15.3 mV/unit change in pH$_i$. Numbers of cells for increasing ΔpH at pH$_i$ 6 = 3, 7, 5, 4; pH$_i$ 7 = 3, 8, 11, 5, 3; and pH$_o$ 7 = 3, 5, 4, 5, 6.

g_H-V relationship (Figs. 3 and 6). Finally, activation kinetics was well described by a single exponential and could not be fitted reasonably with a higher-order function.

There is general agreement that the H$_V$1 dimer in several species gates "cooperatively," but it is less clear what this word means; in drug binding, cooperativity can be produced by quite different mechanisms (Colquhoun, 1973). One sense is that, like the Hodgkin–Huxley model, multiple subunits must move before the channel can conduct. Another sense is that, like oxygen binding to the four hemes of hemoglobin, the movement of one H$_V$1 protomer promotes the movement of the other. The sigmoid activation kinetics of H$_V$1 in several species (Gonzalez et al., 2010; Musset et al., 2010b; Tombola et al., 2010; Fujiwara et al., 2012) appears to reflect that both protomers must undergo a conformational change before either can conduct (first sense; Gonzalez et al., 2010) or highly cooperative gating (second sense; Tombola et al., 2010). When H$_V$1 is forced to exist as a monomer, by splicing it with the N terminus of *Ciona intestinalis* voltage-sensing phosphatase or by truncating the C terminus, the current turns on exponentially and five to seven times faster than with the WT dimeric protein (Koch et al., 2008; Musset et al., 2010a,b; Tombola et al., 2010; Fujiwara et al., 2012). The dimerization of H$_V$1 in several species appears strongly dependent on coiled-coil interactions in the C terminus (Koch et al., 2008; Lee et al., 2008; Tombola et al., 2008; Li et al., 2010). HtH$_V$1 has extensive predicted coiled-coil in its C-terminal region. This complicates the interpretation for HtH$_V$1, because the exponential activation and the apparently first-order kinetics suggest monomeric behavior.

One explanation might be that HtH$_V$1 exists in the membrane as a dimer because of the coiled-coil region, but the coupling between C terminus and S4 segment is dysfunctional, as can be achieved experimentally by introducing a flexible linker between S4 and the C terminus (Fujiwara et al., 2012). However, this appears unlikely to be the case, because the apparent gating charge of HtH$_V$1 is nearly 6 e_0 (5.5 ± 0.9, mean ± SD in a sample of 18 g_H-V curves), based on the limiting slope of the g_H-V relationship. Monomeric H$_V$1 typically exhibit gating charge roughly half that of the dimer, 2–3 versus 4–6 e_0. When the coupling between the C terminus and the S4 helix was disrupted by a flexible linker, the gating charge was halved (Fujiwara et al., 2012). Given that HtH$_V$1 has charged amino acids in its transmembrane regions similar to those of other H$_V$1, we assume that its gating charge has analogous origins. The g_H-V relationships in Fig. 6 J also are compatible with Hodgkin–Huxley-type gating. One possibility is that a concerted rate-limiting step in opening occurs late, presumably after the conformational changes in each monomer (Gonzalez et al., 2010; Musset et al., 2010b; Villalba-Galea, 2014). The voltage-dependent movement of monomers may be so rapid in HtH$_V$1 that the concerted opening step becomes rate limiting. Another speculative explanation for its exponential activation is that HtH$_V$1 enjoys tighter coupling between protomers than H$_V$1 in other species; in essence, both S4 helices move together.

The gating of HtH$_V$1 depends steeply on voltage

Perceptibly different from mammalian H$_V$1, the activation kinetics of snail H$_V$1, HtH$_V$1, is more steeply voltage dependent, giving

a family of currents a distinctive gestalt (Fig. 3 A). In HtH$_V$1, τ_{act} decreased e-fold in 13.8 mV, in contrast to several mammalian H$_V$1, where τ_{act} changes e-fold in 40–72 mV (DeCoursey, 2003). In addition, τ_{tail} increased e-fold in 14.0 mV in HtH$_V$1, compared with a slope typically 26–44 mV/e-fold change in τ_{tail} in mammalian cells (DeCoursey, 2003). The steeply voltage-dependent gating kinetics of HtH$_V$1 is strikingly reminiscent of voltage-gated K$^+$ channel behavior (Cahalan et al., 1985).

Gating kinetics in HtH$_V$1 is strongly dependent on pH$_o$

Byerly et al. (1984) noted that activation kinetics in snail LsH$_V$1 slowed at lower pH$_o$ more than could be accounted for by the shift of the g_H-V relationship. This is clearly true of HtH$_V$1 as well. The τ_{act}-V relationship shifts positively with lower pH$_o$ (Fig. 6 I), but its maximum increases by roughly an order of magnitude per unit decrease in pH$_o$. In stark contrast, in rat H$_V$1, the τ_{act}-V relationship mainly shifted along the voltage axis with changes in pH$_o$, with little change in kinetics. However, the τ_{act}-V relationship in rat was strongly affected by pH$_i$, slowing fivefold per unit increase in pH$_i$ (DeCoursey and Cherny, 1995). In one study of human hH$_V$1, gating was described by three exponentials with activation generally faster at lower pH$_i$ and deactivation faster at higher pH$_i$ (Villalba-Galea, 2014). Qualitatively similar results were reported in mouse macrophages, but the largest change was a two- to threefold slowing of τ_{act} for a 1.5-unit increase in pH$_i$ or a 2.1-unit decrease in pH$_o$ (Kapus et al., 1993). An insect H$_V$1, NpH$_V$1, however, exhibited nearly as strong pH$_o$ dependence of kinetics as found here in HtH$_V$1 (Chaves et al., 2016). In contrast to the strong dependence of activation kinetics on pH$_i$ in rat (DeCoursey and Cherny, 1995), in HtH$_V$1, τ_{act} was in a similar range at all pH$_i$ values from 5 to 8. These differences in gating kinetics among species may make it challenging to produce a single universal model that describes the voltage and pH dependence of gating in all species.

Metal binding site in HtH$_V$1

HtH$_V$1 was moderately sensitive to inhibition by Zn^{2+}, the classic (Thomas and Meech, 1982; Mahaut-Smith, 1989a) and still most potent (Cherny and DeCoursey, 1999) H$_V$1 inhibitor. Somewhat weaker effects were observed for Cd^{2+} (Fig. 5). The principal effects of Zn^{2+} on mammalian H$_V$1 are a slowing of activation, a positive shift of the g_H-V relationship, and possibly a reduction of the maximum H$^+$ conductance, $g_{H,max}$ (Cherny and DeCoursey, 1999). These effects are also observed in HtH$_V$1, but the decrease in $g_{H,max}$ is much more obvious, whereas the shift of the g_H-V relationship is substantially weaker in HtH$_V$1 than in hH$_V$1. Thus, the g_H-V relationship in human hH$_V$1 is shifted more by 1 µM Zn^{2+} (Musset et al., 2010b) than HtH$_V$1 is shifted by 10 µM Zn^{2+} (Fig. 5).

In mammalian H$_V$1, Zn^{2+} binds mainly to two His: His^{140} and His^{193} in hH$_V$1 (Ramsey et al., 2006; Musset et al., 2010b). Surprisingly, when mH$_V$1 was crystallized, it contained a Zn^{2+} atom, coordinated by the corresponding two His with contributions from two acids, Glu^{115} and Asp^{119}, given in Table 1 (Takeshita et al., 2014). Mutation of both acids simultaneously decreases Zn^{2+} affinity of mH$_V$1, but neutralizing either alone does not (Takeshita et al., 2014). As indicated in Table 1, three of these four corresponding residues are conserved in HtH$_V$1: Glu^{114}, Glu^{118} (conservatively replacing Asp), and His^{201}, with Val^{254} replacing the second His. Consistent with the partial conservation of the mammalian Zn^{2+} site, Zn^{2+} was generally less potent in HtH$_V$1 but still quite effective. The main difference in the presumed Zn^{2+} binding residues in HtH$_V$1 is the lack of His^{193}. One might therefore speculate that His^{193} in human hH$_V$1 is important in Zn^{2+} shifting the g_H-V relationship positively. Evidently, when the binding site includes His^{193} located in the external S2–S3 linker, Zn^{2+} binding biases the membrane potential more effectively. Coordination by four amino acids is more typical of a structural Zn^{2+} binding site, whereas catalytic Zn^{2+} binding sites usually have three amino acids and one water as a ligand (Auld, 2001). Of interest is a study showing that the metal transport site of ZnT transporters is selective for Zn^{2+} over Cd^{2+} when the four ligands are 2 His + 2 acids, but cannot discriminate the two metals with 1 His + 3 acids (Hoch et al., 2012). The HtH$_V$1 channel has 1 His + 2 acids and is moderately selective for Zn^{2+} over Cd^{2+}. As shown in Table 1, the NpH$_V$1, CiH$_V$1, CpH$_V$1, SpH$_V$1, and DrH$_V$1 channels share a 1 His + 3 acids scheme and are much less sensitive to Zn^{2+} than mammalian H$_V$1 (Cd^{2+} was not tested) and generally less sensitive than HtH$_V$1. Intriguingly, the D145H mutation in NpH$_V$1 results in 2 His + 2 acids, which markedly increases its Zn^{2+} sensitivity (Chaves et al., 2018). Empirically, Table 1 indicates that the configurations of H$_V$1 for Zn^{2+} binding to H$_V$1 in order of decreasing efficacy are: 2 His + 2 acids > 1 His + 2 acids > 1 His + 3 acids. It appears that the 1 His + 3 acids motif is somewhat less favorable for Zn^{2+} binding than 1 His + 2 acids as found in HtH$_V$1, which seems paradoxical, because the 1 His + 3 acids motif has four ligands instead of three, possibly plus water. Perhaps geometrical factors can be more important than the number of ligands.

The g_H-V relationship of HtH$_V$1 depends more on pH$_o$ and less on pH$_i$ than H$_V$1 in other species

A unique property of H$_V$1 is that its voltage-dependent gating is strongly modulated by pH in a manner called ΔpH dependence (Cherny et al., 1995). The g_H-V relationship is shifted equally by increasing pH$_o$ or decreasing pH$_i$, by –40 mV/unit change, thus responding to the pH gradient (ΔpH) rather than to the absolute pH (Cherny et al., 1995). The practical consequence is that H$_V$1 opens only when the electrochemical gradient for H$^+$ is outward, such that when the channel opens it will always extrude acid from the cell (Doroshenko et al., 1986; DeCoursey and Cherny, 1994). To a rough approximation, all H$_V$1 appear to shift by 40 mV/unit at all pH values (DeCoursey, 2003). Until recently, the rare exceptions to this rule of forty were ignored as anomalies, perhaps reflecting difficulties of the measurements, in particular with control over pH (DeCoursey and Cherny, 1997). However, measurements explicitly addressing this point revealed that the ΔpH-dependent gating of hH$_V$1, kH$_V$1, and EhH$_V$1 does indeed deviate by saturating at high pH, namely above pH$_o$ 8 or pH$_i$ 8 (Cherny et al., 2015). Byerly et al. (1984) reported little shift between pH$_o$ 7.4 and 8.4 in *L. stagnalis*, and this observation is consistent with the saturation at high pH$_o$ observed here for HtH$_V$1 (Fig. 9). The slope in HtH$_V$1 begins to decrease above pH$_o$ 7 (Fig. 9), suggesting that saturation begins at lower pH$_o$ than in

Thomas et al.
A snail proton channel with anomalous properties

Journal of General Physiology
https://doi.org/10.1085/jgp.201711967

847

Table 1. **Putative Zn^{2+}-binding residues in H_V1 from several species**

Species	H_V1 name	Acid$_1$	Acid$_2$	His$_1$	His$_2$	Zn^{2+} potency	Reference
						μM[a]	
Mus musculus	mH$_V$1	Glu^{115}	Asp^{119}	His^{136}	His^{189}	1	Takeshita et al., 2014
Homo sapiens	hH$_V$1	Glu^{119}	Asp^{123}	His^{140}	His^{193}	1	Musset et al., 2010b
Rattus norvegicus	RnH$_V$1	Glu^{115}	Asp^{119}	His^{138}	His^{191}	1	Cherny and DeCoursey, 1999
Helisoma trivolvis	HtH$_V$1	Glu^{114}	Glu^{118}	His^{201}	Val^{254}	10	This study
Nicoletia phytophila	NpH$_V$1	Glu^{73}	Asp^{77}	His^{92}	Asp^{145}	10	Chaves et al., 2018
Ciona intestinalis	CiH$_V$1	Glu^{167}	Asp^{171}	His^{188}	Glu^{243}	10	Qiu et al., 2016
Coccolithus pelagicus	CpH$_V$1	Glu^{80}	Asp^{84}	His^{105}	Glu^{158}	30	Taylor et al., 2011
Strongylocentrotus purpuratus	SpH$_V$1	Glu^{80}	Asp^{84}	His^{114}	Glu^{167}	100	Sakata et al., 2016
Danio rerio	DrH$_V$1	Glu^{84}	Asp^{88}	His^{105}	Asp^{158}	100	Ratanayotha et al., 2017
Lingulodinium polyedrum[b]	LpH$_V$1	Ser^{52}	Glu^{56}	Ala^{161}	Thr^{210}-Asn^{211}	~100	Rodriguez et al., 2017
Emiliania huxleyi[c]	EhH$_V$1	Glu^{117}	Asp^{121}	Thr^{210}	Gly^{298}	~500	Taylor et al., 2011
Karlodinium veneficum	kH$_V$1	Gly^{58}	Glu^{62}	Glu^{109}	Gly^{162}	Weak	DeCoursey, 2012

Acidic amino acids, red; His, aqua; and neutral residues, gray.
[a]Zn^{2+} potency is defined very approximately as the concentration required to shift the g_H-V relationship by 20 mV or reduce current during a test pulse by 50%. The latter is highly arbitrary and depends strongly on the test voltage used (DeCoursey et al., 2001), but in some cases is the only information available. The four amino acids implicated in Zn^{2+} binding were identified in the crystal structure of mH$_V$1, which actually included a bound Zn^{2+} atom, confirmed by mutation of each individually (Takeshita et al., 2014). The importance of the two His in hH$_V$1 have been confirmed in mutation studies (Ramsey et al., 2006; Musset et al., 2010b); all other amino acids in this table are simply located at analogous positions as assessed by multiple alignment.
[b]Given the moderate Zn^{2+} sensitivity of LpH$_V$1, which lacks three of four coordinating groups, it is quite possible that Zn^{2+} binds at a different location.
[c]EhH$_V$1 has two alternatively located His in the S1–S2 linker that bind Zn^{2+} (Taylor et al., 2011).

hH$_V$1. Saturation of ΔpH-dependent gating suggests that pH is approaching the effective pK_a of one or more titratable groups that sense pH$_o$. Given this interpretation, the effective pK_a is roughly 1 unit lower in HtH$_V$1 than in hH$_V$1.

Another deviation from the rule of forty is that the g_H-V relationship in HtH$_V$1 shifted ~60 mV/unit change in pH$_o$ between pH$_o$ 5 and 7 (Fig. 9), well above the classic value of 40 mV/unit change in pH$_o$ (Cherny et al., 1995). This unusual property is shared by several disparate species, including other snails. In *H. pomatia*, the shift was 63 mV from pH$_o$ 7.5 to 6.6 (Doroshenko et al., 1986). In *L. stagnalis*, the shift was 46 mV from pH$_o$ 7.4 to 6.4 (Byerly et al., 1984). Changes in pH$_o$ in a coccolithophore EhH$_V$1 produced shifts of ~50 mV/unit (Cherny et al., 2015). An insect H$_V$1 (NpH$_V$1) shifts 54 mV/unit change in pH$_o$ (Chaves et al., 2016).

More dramatically, changes in pH$_i$ produced much smaller shifts of the g_H-V relationship in HtH$_V$1 than the 40 mV in mammalian species (Cherny et al., 1995). The mean shift in HtH$_V$1 between pH$_i$ 5 and 9 was only 15.3 mV/unit (Fig. 9). This is in remarkable agreement with the 15 mV/unit reported in the snail LsH$_V$1 between pH$_i$ 5.9 and 7.3 (Byerly et al., 1984). Meech (2012) recently emphasized the stronger effects of pH$_o$ over pH$_i$ after reanalyzing old data. However, in another snail, *H. pomatia*, HpH$_V$1 apparently shifted normally, roughly 30–50 mV/unit change in pH$_i$ (Doroshenko et al., 1986), so on this point it is not possible to generalize about molluscan H$_V$1.

The ΔpH dependence of mammalian H$_V$1 results in only outward H$^+$ currents under most circumstances, which is crucial to many if not all of its functions (DeCoursey, 2003). One striking consequence of the anomalous ΔpH dependence of HtH$_V$1 and perhaps of other snail H$_V$1 is that inward currents are readily observed at certain ΔpH. Even at symmetrical pH, there are often inward currents. More conspicuously, because of the weak dependence on pH$_i$, an inward pH gradient (ΔpH < 0) produces inward currents over an extensive voltage range (e.g., Fig. 8 C). Inward currents would affect neuronal excitability by providing a depolarizing current. They at first appear incompatible with an early proposal that proton currents in snail neurons function to extrude protons that enter via Ca^{2+}/H$^+$ exchange after each Ca^{2+}-mediated action potential (Ahmed and Connor, 1980; Thomas and Meech, 1982; Byerly et al., 1984), but under normal conditions of an outward H$^+$ gradient, inward currents would likely not be activated. Nevertheless, the possibility arises that H$_V$1 might mediate action potentials in molluscan neurons under certain conditions, although Ca^{2+} channels are thought to be primarily responsible (Hagiwara and Byerly, 1981). H$_V$1 appears to mediate action potentials in bioluminescent dinoflagellates (Fogel and Hastings, 1972; Smith et al., 2011; Rodriguez et al., 2017).

As *L. stagnalis* and *H. trivolvis* snails live in similar habitats, we expect that their proton channels should function similarly. This view is supported by the similarity of the LsH$_V$1 sequence to that of HtH$_V$1, especially in the S2/S3 region that we have identified for its importance in pH$_i$ sensing in the accompanying paper (Cherny et al., 2018). In that paper, we identify a single amino acid difference between hH$_V$1 and HtH$_V$1 that appears largely responsible for the difference in pH$_i$ sensing.

Acknowledgments

References

Ahmed, Z., and J.A. Connor. 1980. Intracellular pH changes induced by calcium influx during electrical activity in molluscan neurons. *J. Gen. Physiol.* 75:403–426. https://doi.org/10.1085/jgp.75.4.403

Auld, D.S. 2001. Zinc coordination sphere in biochemical zinc sites. *Biometals.* 14:271–313. https://doi.org/10.1023/A:1012976615056

Bernheim, L., R.M. Krause, A. Baroffio, M. Hamann, A. Kaelin, and C.R. Bader. 1993. A voltage-dependent proton current in cultured human skeletal muscle myotubes. *J. Physiol.* 470:313–333. https://doi.org/10.1113/jphysiol.1993.sp019860

Byerly, L., R. Meech, and W. Moody Jr. 1984. Rapidly activating hydrogen ion currents in perfused neurones of the snail, *Lymnaea stagnalis. J. Physiol.* 351:199–216. https://doi.org/10.1113/jphysiol.1984.sp015241

Cahalan, M.D., K.G. Chandy, T.E. DeCoursey, and S. Gupta. 1985. A voltage-gated potassium channel in human T lymphocytes. *J. Physiol.* 358:197–237. https://doi.org/10.1113/jphysiol.1985.sp015548

Chaves, G., C. Derst, A. Franzen, Y. Mashimo, R. Machida, and B. Musset. 2016. Identification of an H_V1 voltage-gated proton channel in insects. *FEBS J.* 283:1453–1464. https://doi.org/10.1111/febs.13680

Chaves, G., S. Bungert-Plümke, A. Franzen, and B. Musset. 2018. Zinc inhibition of an insect voltage-gated proton channel. *Biophys. J.* 114:492a. https://doi.org/10.1016/j.bpj.2017.11.2697

Cherny, V.V., and T.E. DeCoursey. 1999. pH-dependent inhibition of voltage-gated H^+ currents in rat alveolar epithelial cells by Zn^{2+} and other divalent cations. *J. Gen. Physiol.* 114:819–838. https://doi.org/10.1085/jgp.114.6.819

Cherny, V.V., V.S. Markin, and T.E. DeCoursey. 1995. The voltage-activated hydrogen ion conductance in rat alveolar epithelial cells is determined by the pH gradient. *J. Gen. Physiol.* 105:861–896. https://doi.org/10.1085/jgp.105.6.861

Cherny, V.V., L.L. Thomas, and T.E. DeCoursey. 2001. Voltage-gated proton currents in human basophils. *Биол. мембраны.* 18:458–465.

Cherny, V.V., D. Morgan, B. Musset, G. Chaves, S.M.E. Smith, and T.E. DeCoursey. 2015. Tryptophan 207 is crucial to the unique properties of the human voltage-gated proton channel, hH_V1. *J. Gen. Physiol.* 146:343–356.

Cherny, V.V., D. Morgan, S. Thomas, S.M.E. Smith, and T.E. DeCoursey. 2018. Histidine[168] is crucial for ΔpH-dependent gating of the human voltage-gated proton channel, hH_V1. *J. Gen. Physiol.* https://doi.org/10.1085/jgp.201711968

Cohan, C.S., J.L. Karnes, and F.Q. Zhou. 2003. Culturing neurons from the snail *Helisoma. Methods Cell Biol.* 71:157–170. https://doi.org/10.1016/S0091-679X(03)01009-4

Colquhoun, D. 1973. The relation between classical and cooperative models for drug action. *In* Drug Receptors. H.P. Rang, editor. Palmgrave, London. 149–182. https://doi.org/10.1007/978-1-349-00910-7_11.

DeCoursey, T.E. 1991. Hydrogen ion currents in rat alveolar epithelial cells. *Biophys. J.* 60:1243–1253. https://doi.org/10.1016/S0006-3495(91)82158-0

DeCoursey, T.E. 2003. Voltage-gated proton channels and other proton transfer pathways. *Physiol. Rev.* 83:475–579. https://doi.org/10.1152/physrev.00028.2002

DeCoursey, T.E. 2012. Voltage-gated proton channels. *Compr. Physiol.* 2:1355–1385. https://doi.org/10.1002/cphy.c100071

DeCoursey, T.E. 2013. Voltage-gated proton channels: molecular biology, physiology, and pathophysiology of the H_V family. *Physiol. Rev.* 93:599–652. https://doi.org/10.1152/physrev.00011.2012

DeCoursey, T.E. 2016. The intimate and controversial relationship between voltage-gated proton channels and the phagocyte NADPH oxidase. *Immunol. Rev.* 273:194–218. https://doi.org/10.1111/imr.12437

DeCoursey, T.E., and V.V. Cherny. 1993. Potential, pH, and arachidonate gate hydrogen ion currents in human neutrophils. *Biophys. J.* 65:1590–1598. https://doi.org/10.1016/S0006-3495(93)81198-6

DeCoursey, T.E., and V.V. Cherny. 1994. Voltage-activated hydrogen ion currents. *J. Membr. Biol.* 141:203–223. https://doi.org/10.1007/BF00235130

DeCoursey, T.E., and V.V. Cherny. 1995. Voltage-activated proton currents in membrane patches of rat alveolar epithelial cells. *J. Physiol.* 489:299–307. https://doi.org/10.1113/jphysiol.1995.sp021051

DeCoursey, T.E., and V.V. Cherny. 1996. Voltage-activated proton currents in human THP-1 monocytes. *J. Membr. Biol.* 152:131–140. https://doi.org/10.1007/s002329900092

DeCoursey, T.E., and V.V. Cherny. 1997. Deuterium isotope effects on permeation and gating of proton channels in rat alveolar epithelium. *J. Gen. Physiol.* 109:415–434. https://doi.org/10.1085/jgp.109.4.415

DeCoursey, T.E., V.V. Cherny, A.G. DeCoursey, W. Xu, and L.L. Thomas. 2001. Interactions between NADPH oxidase-related proton and electron currents in human eosinophils. *J. Physiol.* 535:767–781. https://doi.org/10.1111/j.1469-7793.2001.00767.x

Delorenzi, M., and T. Speed. 2002. An HMM model for coiled-coil domains and a comparison with PSSM-based predictions. *Bioinformatics.* 18:617–625. https://doi.org/10.1093/bioinformatics/18.4.617

Demaurex, N., S. Grinstein, M. Jaconi, W. Schlegel, D.P. Lew, and K.H. Krause. 1993. Proton currents in human granulocytes: regulation by membrane potential and intracellular pH. *J. Physiol.* 466:329–344.

Doroshenko, P.A., P.G. Kostyuk, and A.E. Martynyuk. 1986. Transmembrane outward hydrogen current in intracellularly perfused neurones of the snail *Helix pomatia. Gen. Physiol. Biophys.* 5:337–350.

Fogel, M., and J.W. Hastings. 1972. Bioluminescence: mechanism and mode of control of scintillon activity. *Proc. Natl. Acad. Sci. USA.* 69:690–693. https://doi.org/10.1073/pnas.69.3.690

Fujiwara, Y., T. Kurokawa, K. Takeshita, M. Kobayashi, Y. Okochi, A. Nakagawa, and Y. Okamura. 2012. The cytoplasmic coiled-coil mediates cooperative gating temperature sensitivity in the voltage-gated H^+ channel Hv1. *Nat. Commun.* 3:816. https://doi.org/10.1038/ncomms1823

Gonzalez, C., H.P. Koch, B.M. Drum, and H.P. Larsson. 2010. Strong cooperativity between subunits in voltage-gated proton channels. *Nat. Struct. Mol. Biol.* 17:51–56. https://doi.org/10.1038/nsmb.1739

Gonzalez, C., S. Rebolledo, M.E. Perez, and H.P. Larsson. 2013. Molecular mechanism of voltage sensing in voltage-gated proton channels. *J. Gen. Physiol.* 141:275–285. https://doi.org/10.1085/jgp.201210857

Hagiwara, S., and L. Byerly. 1981. Calcium channel. *Annu. Rev. Neurosci.* 4:69–125. https://doi.org/10.1146/annurev.ne.04.030181.000441

Hille, B. 2001. Ion Channels of Excitable Membranes. Third edition. Sinauer Associates, Sunderland, MA. 814 pp.

Hoch, E., W. Lin, J. Chai, M. Hershfinkel, D. Fu, and I. Sekler. 2012. Histidine pairing at the metal transport site of mammalian ZnT transporters controls Zn^{2+} over Cd^{2+} selectivity. *Proc. Natl. Acad. Sci. USA.* 109:7202–7207. https://doi.org/10.1073/pnas.1200362109

Hodgkin, A.L., and A.F. Huxley. 1952. A quantitative description of membrane current and its application to conduction and excitation in nerve. *J. Physiol.* 117:500–544. https://doi.org/10.1113/jphysiol.1952.sp004764

Imperiali, B., and S.E. O'Connor. 1999. Effect of N-linked glycosylation on glycopeptide and glycoprotein structure. *Curr. Opin. Chem. Biol.* 3:643–649. https://doi.org/10.1016/S1367-5931(99)00021-6

Kapus, A., R. Romanek, A.Y. Qu, O.D. Rotstein, and S. Grinstein. 1993. A pH-sensitive and voltage-dependent proton conductance in the plasma membrane of macrophages. *J. Gen. Physiol.* 102:729–760. https://doi.org/10.1085/jgp.102.4.729

Kater, S.B. 1974. Feeding in *Helisoma trivolvis*: The morphological and physiological bases of a fixed action pattern. *Am. Zool.* 14:1017–1036. https://doi.org/10.1093/icb/14.3.1017

Koch, H.P., T. Kurokawa, Y. Okochi, M. Sasaki, Y. Okamura, and H.P. Larsson. 2008. Multimeric nature of voltage-gated proton channels. *Proc. Natl. Acad. Sci. USA.* 105:9111–9116. https://doi.org/10.1073/pnas.0801553105

Lee, S.Y., J.A. Letts, and R. Mackinnon. 2008. Dimeric subunit stoichiometry of the human voltage-dependent proton channel Hv1. *Proc. Natl. Acad. Sci. USA.* 105:7692–7695. https://doi.org/10.1073/pnas.0803277105

Li, Q., R. Shen, J.S. Treger, S.S. Wanderling, W. Milewski, K. Siwowska, F. Bezanilla, and E. Perozo. 2015. Resting state of the human proton channel dimer in a lipid bilayer. *Proc. Natl. Acad. Sci. USA.* 112:E5926–E5935. https://doi.org/10.1073/pnas.1515043112

Li, S.J., Q. Zhao, Q. Zhou, H. Unno, Y. Zhai, and F. Sun. 2010. The role and structure of the carboxyl-terminal domain of the human voltage-gated proton channel Hv1. *J. Biol. Chem.* 285:12047–12054. https://doi.org/10.1074/jbc.M109.040360

Mahaut-Smith, M.P. 1989a. The effect of zinc on calcium and hydrogen ion currents in intact snail neurones. *J. Exp. Biol.* 145:455–464.

Mahaut-Smith, M.P. 1989b. Separation of hydrogen ion currents in intact molluscan neurones. *J. Exp. Biol.* 145:439–454.

Meech, R. 2012. A contribution to the history of the proton channel. *Wiley Interdiscip. Rev. Membr. Transp. Signal.* 1:533–557. https://doi.org/10.1002/wmts.59

Musset, B., S.M.E. Smith, S. Rajan, V.V. Cherny, D. Morgan, and T.E. DeCoursey. 2010a. Oligomerization of the voltage-gated proton channel. *Channels (Austin).* 4:260–265. https://doi.org/10.4161/chan.4.4.12789

Musset, B., S.M.E. Smith, S. Rajan, V.V. Cherny, S. Sujai, D. Morgan, and T.E. DeCoursey. 2010b. Zinc inhibition of monomeric and dimeric proton channels suggests cooperative gating. *J. Physiol.* 588:1435–1449. https://doi.org/10.1113/jphysiol.2010.188318

Musset, B., S.M.E. Smith, S. Rajan, D. Morgan, V.V. Cherny, and T.E. DeCoursey. 2011. Aspartate 112 is the selectivity filter of the human voltage-gated proton channel. *Nature.* 480:273–277. https://doi.org/10.1038/nature10557

Qiu, F., A. Chamberlin, B.M. Watkins, A. Ionescu, M.E. Perez, R. Barro-Soria, C. González, S.Y. Noskov, and H.P. Larsson. 2016. Molecular mechanism of Zn^{2+} inhibition of a voltage-gated proton channel. *Proc. Natl. Acad. Sci. USA.* 113:E5962–E5971. https://doi.org/10.1073/pnas.1604082113

Ramsey, I.S., M.M. Moran, J.A. Chong, and D.E. Clapham. 2006. A voltage-gated proton-selective channel lacking the pore domain. *Nature.* 440:1213–1216. https://doi.org/10.1038/nature04700

Ramsey, I.S., Y. Mokrab, I. Carvacho, Z.A. Sands, M.S.P. Sansom, and D.E. Clapham. 2010. An aqueous H^+ permeation pathway in the voltage-gated proton channel Hv1. *Nat. Struct. Mol. Biol.* 17:869–875. https://doi.org/10.1038/nsmb.1826

Ratanayotha, A., T. Kawai, S.I. Higashijima, and Y. Okamura. 2017. Molecular and functional characterization of the voltage-gated proton channel in zebrafish neutrophils. *Physiol. Rep.* 5:e13345. https://doi.org/10.14814/phy2.13345

Rodriguez, J.D., S. Haq, T. Bachvaroff, K.F. Nowak, S.J. Nowak, D. Morgan, V.V. Cherny, M.M. Sapp, S. Bernstein, A. Bolt, et al. 2017. Identification of a vacuolar proton channel that triggers the bioluminescent flash in dinoflagellates. *PLoS One.* 12:e0171594. https://doi.org/10.1371/journal.pone.0171594

Sakata, S., N. Miyawaki, T.J. McCormack, H. Arima, A. Kawanabe, N. Özkucur, T. Kurokawa, Y. Jinno, Y. Fujiwara, and Y. Okamura. 2016. Comparison between mouse and sea urchin orthologs of voltage-gated proton channel suggests role of S3 segment in activation gating. *Biochim. Biophys. Acta.* 1858:2972–2983. https://doi.org/10.1016/j.bbamem.2016.09.008

Sasaki, M., M. Takagi, and Y. Okamura. 2006. A voltage sensor-domain protein is a voltage-gated proton channel. *Science.* 312:589–592. https://doi.org/10.1126/science.1122352

Schilling, T., A. Gratopp, T.E. DeCoursey, and C. Eder. 2002. Voltage-activated proton currents in human lymphocytes. *J. Physiol.* 545:93–105. https://doi.org/10.1113/jphysiol.2002.028878

Smith, S.M.E., D. Morgan, B. Musset, V.V. Cherny, A.R. Place, J.W. Hastings, and T.E. DeCoursey. 2011. Voltage-gated proton channel in a dinoflagellate. *Proc. Natl. Acad. Sci. USA.* 108:18162–18167. https://doi.org/10.1073/pnas.1115405108

Takeshita, K., S. Sakata, E. Yamashita, Y. Fujiwara, A. Kawanabe, T. Kurokawa, Y. Okochi, M. Matsuda, H. Narita, Y. Okamura, and A. Nakagawa. 2014. X-ray crystal structure of voltage-gated proton channel. *Nat. Struct. Mol. Biol.* 21:352–357. https://doi.org/10.1038/nsmb.2783

Taylor, A.R., A. Chrachri, G. Wheeler, H. Goddard, and C. Brownlee. 2011. A voltage-gated H^+ channel underlying pH homeostasis in calcifying coccolithophores. *PLoS Biol.* 9:e1001085. https://doi.org/10.1371/journal.pbio.1001085

Thomas, R.C., and R.W. Meech. 1982. Hydrogen ion currents and intracellular pH in depolarized voltage-clamped snail neurones. *Nature.* 299:826–828. https://doi.org/10.1038/299826a0

Tombola, F., M.H. Ulbrich, and E.Y. Isacoff. 2008. The voltage-gated proton channel Hv1 has two pores, each controlled by one voltage sensor. *Neuron.* 58:546–556. https://doi.org/10.1016/j.neuron.2008.03.026

Tombola, F., M.H. Ulbrich, S.C. Kohout, and E.Y. Isacoff. 2010. The opening of the two pores of the Hv1 voltage-gated proton channel is tuned by cooperativity. *Nat. Struct. Mol. Biol.* 17:44–50. https://doi.org/10.1038/nsmb.1738

Villalba-Galea, C.A. 2014. Hv1 proton channel opening is preceded by a voltage-independent transition. *Biophys. J.* 107:1564–1572. https://doi.org/10.1016/j.bpj.2014.08.017